International Journal of Computer Information Systems and Industrial Management Applications
ISSN 2150-7988 Volume 18 (2026) pp. 1-14
© Cerebration Science Publishing
https://doi.org/10.70917/ijcisim-2026-1813
Article

Improved nicr-nisi thin-film thermocouple manufacturing process enables accurate temperature measurement of UAV engines

Jiayi Sun[1,*]

[1] School of Materials Science and Engineering, Northeast University, Shenyang, Liaoning, 110004, China
* Correspondence author: 15754546025@163.com

Abstract: UAV engine turbine blade temperature measurement is an important basis for its working condition monitoring and health management, and high-temperature thin film thermocouple is considered to be an effective method to solve the problem of its temperature measurement in extreme environment. In this paper, the K-type NiCr-NiSi thin film thermocouple is taken as the research object, and the NiCr-NiSi thin film thermocouple is prepared on Ni-based superalloy substrate using electron beam evaporation and magnetron sputtering, and the improved thin film thermocouple consists of the Ni-based superalloy substrate, the NiCrAlY transition layer, the Al_2O_3 thermal oxide layer, alumina insulating layer, NiCr-NiSi thin-film thermocouple layer, and alumina protective layer. The results of calibration and compositional tests of the thin film thermocouple samples show that the improved NiCr-NiSi thin film thermocouple has a good linearity of Seebeck coefficient of 40.5 μV/K in 50~650 ℃, which is slightly lower than that of the standard thermocouple of type K with Seebeck coefficient of 41.0 μV/K. The dynamic performance of the temperature sensors has been investigated and tested both theoretically and experimentally, and the theoretical and experimental performance of the thermocouple has been investigated and tested. The dynamic performance of the temperature sensor was investigated and tested from both theoretical and experimental points of view. The theoretically calculated time constant was 38.5 μs, and the experimentally tested time constant was 85.05 us, with the response time in the same order of magnitude. The temperature measurement performance of the temperature sensor tested in a constant temperature field can meet the temperature testing requirements in the environment of up to 650°C, and can be reliably applied to the accurate temperature measurement of UAV engines.

Keywords: thin film thermocouple; NiCr-NiSi; calibration test; Seebeck coefficient; temperature sensor

1. Introduction

UAV engine belongs to one kind of aviation power, whether it is piston engine or turbojet engine, it has a more compact construction, smaller volume size and lighter own weight, which not only makes the engine easy to install in use, but more importantly reduces the takeoff burden in the application of aviation power [1-3]. In order to avoid damage to the engine caused by high temperature, engine temperature measurement has become an important measure to determine the health status of the engine [4-5].

Currently, although a variety of thermal sensors have been developed for high-temperature measurement, such as thermocouples, infrared sensors, optical sensors, etc., inside the engine, the environmental conditions are extremely harsh, so a method that can accurately measure the temperature in a high-temperature harsh environment is needed. Thin-film thermocouple heat has the advantages of small capacity, fast thermoelectric response, resistance to spalling, excellent resistance to thermal shock, and little interference with the working environment, which can be used in the work of accurate temperature measurement in UAV engines [6-7]. And nickel-chromium-nickel-silicon (nicr-nisi) thin film thermocouples can realize faster thermal response and smaller space occupation because of high

Copyright: © 2026 by the authors

thermoelectric potential rate and lower cost [8-9]. However, the manufacturing process of nicr-nisi thin film thermocouples still suffers from insufficient strength under extreme conditions such as strong vibration and thermal shock of UAV engines, which limits the accuracy of temperature measurement in UAV engines [10-12]. Therefore, improving the manufacturing process of nicr-nisi thin-film thermocouples is of great practical significance for realizing accurate UAV engine temperature measurement [13-14].

This paper theoretically reveals the optimal compositional ratio compositional origin of binary solid solution alloys commonly used in the field of thermocouples. An improved K-type NiCr-NiSi thin-film thermocouple was fabricated in-house by electron beam evaporation and magnetron sputtering. It consists of a Ni-based superalloy substrate, NiCrAlY transition layer, Al_2O_3 thermal oxide layer, alumina insulating layer, NiCr-NiSi thin-film thermocouple layer, and alumina protective layer. The static and dynamic properties of the NiCr/NiSi thin-film thermocouple were investigated, and the temperature measurement experiments of the high-temperature transient temperature sensors prepared on the surface of the NiCr-NiSi composite material were carried out using a FULKE9144 dry metering furnace as a stable heat source.

2. Methodology

2.1. Thin Film Thermocouples

2.1.1. Principle of operation

Thin film thermocouple working principle is based on the thermoelectric effect, the principle is shown in Figure 1, the A, B two different materials conductor connected to the loop, when the temperature of the hot end and the cold end temperature temperature temperature difference, the material due to the movement of the electrons will produce a thermoelectric potential. The use of thermoelectric effect temperature measurement, the cold end of the lead is usually connected to the voltage collector to collect the thermal voltage, and then through the static calibration to get the temperature of the hot end (the temperature of the cold end is fixed) and the thermoelectric output of the linear relationship between the inverse of the measured temperature value.

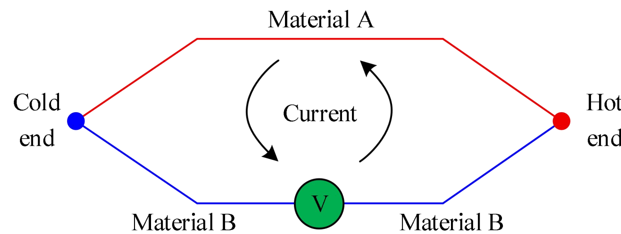

Figure 1. A thermocouple composed of two conductors and temperature measurement

When two conductor materials combined into a thermocouple, hot and cold ends were in the same temperature field, due to different materials, two materials in the cold end of the potential will be different, this potential difference is called the temperature difference electric potential. When the two ends of the same conductor in different temperature field T_1, $T_0\left(T_1 > T_0\right)$, A, B two different conductor materials in this temperature field generated by its own temperature difference potential is calculated as follows:

$$E_A(T_0,T_1)=\int_{T_0}^{T_1}\sigma_A(T_1)dT \tag{1}$$

$$E_B(T_0,T_1)=\int_{T_0}^{T_1}\sigma_B(T_1)dT \tag{2}$$

$$E_A(T_0,T_1)-E_B(T_0,T_1)=\int_{T_0}^{T_1}\left(\sigma_A-\sigma_B\right)dT \tag{3}$$

where σ_A, σ_B - Thomson's coefficient.

Equation (1) and (2) for A, B two materials temperature difference potential, equation (3) obtained by the difference in electric potential that is one of the sources of thermocouple thermal electric potential. From the formula (3) can be seen, if the choice of two identical conductor materials,

then the material itself has the same properties, the composition of the thermocouple will not produce temperature difference potential.

The contact electromotive force is another source of the thermal electromotive force that makes up the thermocouple, as shown in Figure 2. Due to the different basic material properties of the two conductors, there are differences in the free electrons within the materials. When conductors A and B are in contact, free electrons move from the denser end to the less dense end. The end that gains electrons is negatively charged and the end that loses electrons is positively charged, so a potential difference is formed on the contact surface.

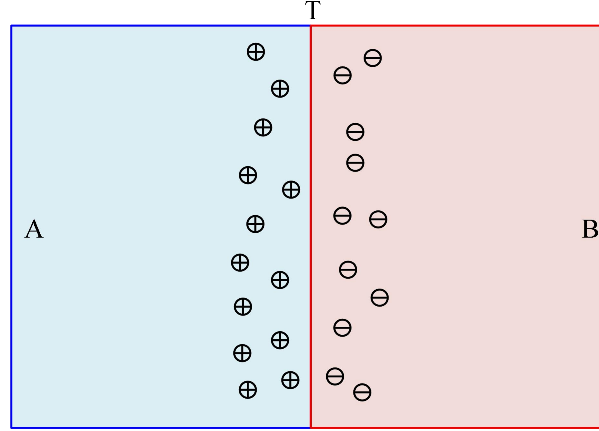

Figure 2. Schematic diagram of contact electromotive force

In the thermocouple circuit, when A, B two different conductor material ends are in the T_0, T_1 temperature, and T_1 is greater than T_0, the conductor of different temperature ends of the contact potential can be expressed as:

$$E_{AB}(T_0)=\frac{kT_0}{e}\ln\frac{n_A}{n_B} \tag{4}$$

$$E_{AB}(T_1)=\frac{kT_1}{e}\ln\frac{n_A}{n_B} \tag{5}$$

The total contact potential in the loop is the difference between equations (4) and (5):

$$E_{AB}(T_1)-E_{AB}(T_0)=\frac{kT_1}{e}\ln\frac{n_A}{n_B}-\frac{kT_0}{e}\ln\frac{n_A}{n_B}=\frac{k}{e}(T_1-T_0)\ln\frac{n_A}{n_B} \tag{6}$$

where, k - Boltzmann's constant;

e - electron charge;

n_A - material A free electron concentration;

n_B - material B free electron concentration.

From equation (6), it can be seen that the source of the contact electric potential is closely related to the temperature difference and the free electron concentration of the two conductor materials. In the circuit, when the temperature of the hot and cold ends is the same, or the carrier concentration of the conductor materials is the same, then the contact electric potential is also zero. Combined with the above formula (3) and (6) analysis, the total thermal electric potential of the thermocouple is the sum of the two electric potentials. The total electric potential is calculated as follows:

$$E_{AB}(T_1,T_0)=\int_{T_0}^{T_1}(\sigma_A-\sigma_B)dT+\frac{k}{e}(T_1-T_0)\ln\frac{n_A}{n_B} \tag{7}$$

From equation (7), it can be seen that the decision of the total potential difference size is only related to the two conductors themselves material properties and the temperature of the hot and cold ends of the circuit. When the temperature difference between the hot and cold ends is zero, the circuit potential difference is zero. When the same conductor material, due to the same material properties of their own parameters, the potential difference is also zero. Equation (7) can be transformed into the

following formula:

$$E_{AB}(T_1,T_0)=\int_{T_0}^{T_1}\left[\frac{k}{e}\ln\frac{n_A}{n_B}+(\sigma_A-\sigma_B)\right]dT=\int_{T_0}^{T_1}S_{AB}dT \tag{8}$$

where, S_{AB} - thermocouple sensitivity coefficient / $\mu\text{V}/^{\circ}\text{C}$.

From the formula (8) can be seen, after the election of the two conductor materials, the basic characteristics of the material is also determined, the thermocouple sensitivity coefficient S_{AB} basically a fixed value. At this time the sensor's voltage output is only a single-valued function of temperature. The thermopotential can be expressed as:

$$E_{AB}(T_1,T_0)=S_{AB}(T_1-T_0) \tag{9}$$

When the cold end temperature is room temperature or known to be a constant value, then the thermoelectric output of the thermocouple is only related to the measured temperature. After selecting a good thermoelectric material, the sensitivity coefficients of the thermocouple are determined so that thermocouples with a thermoelectric effect can be calibrated for temperature measurement.

2.1.2. Important laws

(1) Law of homogeneous conductors

When the same homogeneous conductor material is used to form a thermocouple, regardless of the size of the two conductor materials, the shape of the size and the temperature field is different, there will be no thermal potential output in the loop. From the principle of temperature difference electric potential, the same conductor material has the same Thomson's coefficient and the same material properties. Therefore, they cannot be used to form a thermocouple. Emphasize the homogeneous conductor is because the default conductor material internal basic properties of uniformity, otherwise there will be additional thermal potential in the temperature difference, resulting in temperature measurement deviation.

(2) Law of intermediate conductors

Add a section of conductor material C at the cold end of the thermocouple and make sure that the temperature values at both connection locations are T_0, and by the law of intermediate conductors, the accessed conductor material C will not have an effect on the original thermocouple circuit. The calculation process is as follows. When the conductor material C is added, the total thermal potential in the loop is:

$$\begin{aligned}E_{ABC}(T,T_0)&=E_{AB}(T)+E_{BC}(T_0)+E_{CA}(T_0)+E_B(T,T_0)\\&+E_C(T_0,T_0)+E_A(T_0,T)\end{aligned} \tag{10}$$

Assuming that the conductor C has the same temperature as the thermocouple connection, both are T_0, as shown by the previous analysis:

$$E_{ABC}(T_0)=E_{AB}(T_0)+E_{BC}(T_0)+E_{CA}(T_0)=0 \tag{11}$$

$$E_{BC}(T_0)+E_{CA}(T_0)=-E_{AB}(T_0) \tag{12}$$

Substituting $E_C(T_0,T_0)=0$ and Eq. (12) into Eq. (10) gives:

$$\begin{aligned}E_{ABC}(T,T_0)&=E_{AB}(T)-E_{AB}(T_0)+E_B(T,T_0)+E_A(T_0,T)\\&=E_{AB}(T)-E_{AB}(T_0)+E_B(T,T_0)-E_A(T,T_0)\\&=E_{AB}(T,T_0)\end{aligned} \tag{13}$$

It can be seen that the law of intermediate conductors is the basis for thermocouple extension wires. In practice, the thermocouple hot end may use high-temperature resistant precious metal materials, while the cold end interface will generally be extended to room temperature, if the thermocouple all the use of precious metals is too costly, and therefore the need for a third, cheaper conductor material to extend the wire. When the temperature of the access point is the same, there will be no effect on the total potential of the loop.

(3) Law of Intermediate Temperatures

When the cold end of the original thermocouple interface are connected to the other two conductor materials, and access point temperature is the same. Then the total electric potential in the loop is the

thermal potential E_{AB} plus the potential generated by the back-end wires $E_{A'B'}$, the law of intermediate temperatures is also very commonly used in in practice, also to save the cost of the thermoelectric material, at the cold end is often connected to the cold end of the cold end of the extension cord with the precious metal thermocouple to match.

(4) Reference electrode law

When two conductors A and B are respectively combined with the third conductor C to form AC and BC thermocouples, the temperatures at the cold and hot ends of the thermocouples are T and T_0 respectively. The thermoelectric voltages in the two thermocouple circuits are $E_{AC}(T,T_0)$ and $E_{BC}(T,T_0)$ respectively. If the two thermocouples are connected in series, then $E_{AB}(T,T_0)$ can be expressed as:

$$E_{AB}(T,T_0) = E_{AC}(T,T_0) + E_{BC}(T,T_0) \tag{14}$$

The law of reference electrode is often used to calibrate the thermoelectric material, selected conductor material C as the standard electrode, other conductor material by forming a thermocouple with the standard material and static calibration, you can know the Seebeck coefficient of this material. Thus, it is convenient to evaluate the thermoelectric properties of any two conductor materials and to judge the advantages and disadvantages of their composition of thermocouples.

2.2. Thin Film Preparation and Characterization Techniques

2.2.1. Film Preparation Technology

According to the difference in the principle of preparation technology, thin film preparation technology can be divided into two categories: physical and chemical methods. Physical methods usually involve the transfer of material atoms to the surface of the substrate material through physical processes such as thermal evaporation or sputtering of atoms on the surface of the material by particle bombardment, which mainly include evaporation, sputtering, and so on. The chemical method is usually through the gas flow will contain thin film material composition of liquid or gaseous reactant introduced into the process chamber, followed by a chemical reaction on the substrate surface, so as to deposit thin films, which includes CVD, ALD, sol-gel method, etc..

(1) Magnetron sputtering technology

Magnetron sputtering technology is one of the main methods of physical vapor deposition, which can realize high-speed deposition under the conditions of low temperature and low damage, and can be traced back to the 1930s. Because magnetron sputtering has many advantages such as fast deposition speed, small damage to the film layer, uniform and dense film layer, high purity and wide application of target materials, magnetron sputtering technology has been rapidly developed and improved.

Figure 3 is the working principle diagram of magnetron sputtering. A magnet is placed at the bottom of the target material (cathode) to form a magnetic field parallel to the surface of the target. When a voltage is applied, electrons move at high speed through the Cu plate above the magnet and escape from the target surface. They collide with rare gas atoms such as Ar atoms introduced into the chamber, ionizing Ar^+ and secondary electrons, forming a plasma and causing a "glow phenomenon". The Ar^+ ions ionized by this process are accelerated by the circular magnetic field track and bombard the target material. The target atoms impacted gain energy and condense onto the substrate (anode) surface to form a film.

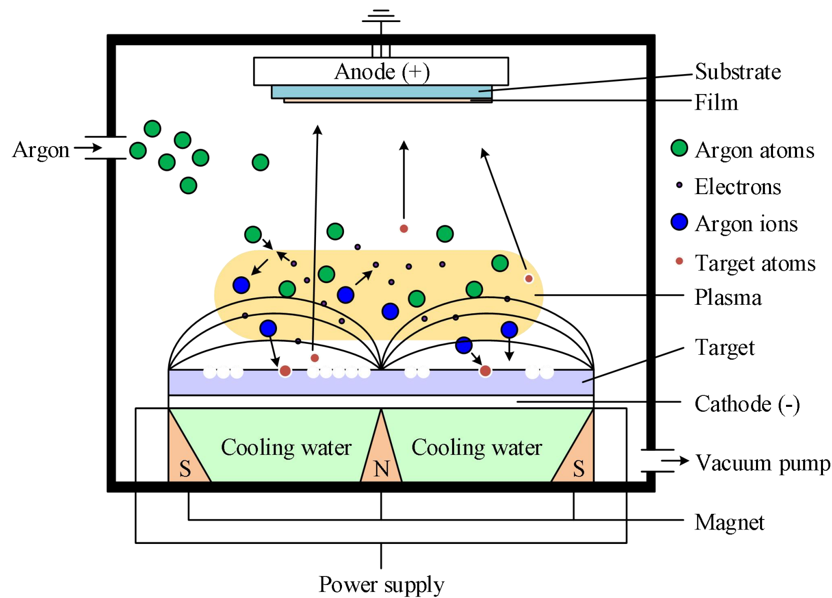

Figure 3. Schematic diagram of magnetron sputtering

(2) Atomic Layer Deposition

Atomic Layer Deposition (ALD) technology is a chemical vapor deposition method for thin films based on a self-limiting reaction, which has a number of advantages over other physical or chemical deposition techniques, such as simplicity, reproducibility, and a high degree of control over the film composition and thickness, which allows for precise control of the film growth down to the single-atom level. A self-limiting reaction is one in which a reactant is adsorbed onto a substrate and a second or third gas enters the chamber and chemisorbs with the substrate to form a thin film, a reaction that occurs only at the reactant and the surface.ALD technology is based on the principle of pulsing different source vapors alternately into the vacuum reaction chamber, one at a time, separated by a purge or evacuation cycle, where the different reactants adsorb on the surface of the substrate and undergo a chemical reaction that produces a thin film.

2.2.2. Thin Film Characterization Techniques

Thin film characterization techniques allow in-depth study of the microstructure and composition of thin films to optimize the film preparation process. In this paper, we mainly use scanning electron microscope (SEM), energy spectrometer (EDS), step meter and four-probe tester to characterize and analyze a variety of thin films prepared.

(1) Scanning Electron Microscope

Scanning electron microscope is an important means of thin film characterization, this paper uses SEM to characterize the cross-section, surface microstructure and morphology of the film. Its working principle is to use a fine focused electron beam, under the action of the deflection coil in the film surface to do grating scanning, electron interaction with the film surface will produce secondary electrons, backscattered electrons and other characteristics of the signal, the detector collects the signal after computer processing can display the electronic image of the film surface or cross-section can be observed and analyzed.

(2) Spectrometer

An energy spectrometer is an instrument used to analyze the composition of materials and the distribution of elements, usually in conjunction with a scanning electron microscope and a transmission electron microscope. It can not only obtain the microscopic morphology of a thin film, but also analyze the elemental species and elemental distribution in specific areas of the film, such as (points, lines and surfaces). The principle is to bombard the surface of the film with an electron beam, which excites the electrons in the inner layer of the material to emit specific wavelengths of X rays, and based on the wavelengths, it can be analyzed to determine the composition and specific gravity of the elements in the region.

(3) Stage Meter

A step meter is used to scan the surface of a film by sliding a stylus along the surface of the film to be measured. The stylus will move up and down along the peaks and valleys of the film surface, and changes in displacement can be detected according to the movement. Precise control of film thickness

is an important issue in the process of film preparation. Preparation of films with a step structure can quickly and accurately measure the film thickness and improve the preparation efficiency.

(4) Four-probe tester

The four-probe method is one of the most commonly used methods for measuring resistivity. It usually consists of four equally spaced metal probes arranged in a zigzag pattern, with the probes placed vertically on the film surface, and a constant current source applies a suitable current I to the left and right probes, and then the voltage V between the two middle probes can be measured. The square resistance is obtained from the measurement results, and the resistivity is calculated from the thickness.

2.3. Improved NiCr-NiSi film preparation

Figure 4 shows the structure of the metal-based NiCr-NiSi thin-film thermocouple studied in this paper, and the substrate is made of Ni-based superalloy (DZ4). As the substrate is a conductive metal, it is necessary to deposit an alumina electric insulating layer on the surface of the metal substrate, so as to avoid the conductive metal substrate to interfere with the measurement of the electrical signal generated by the thermocouple. However, due to the large difference in the coefficient of thermal expansion between the alumina and the Ni-based superalloy, the insulating layer is easily removed when heated. Therefore, it is necessary to prepare a transition layer of NiCrAlY alloy on a metal substrate first, and the NiCrAlY transition layer precipitates a layer of metal Al on the surface by vacuum heat treatment, and then generates a layer of alumina on the surface by thermal oxidation process. In order to prevent the NiCr-NiSi layer oxidation at high temperatures affect the performance of the thermocouple, the thermocouple surface needs to deposit a layer of alumina protective layer.

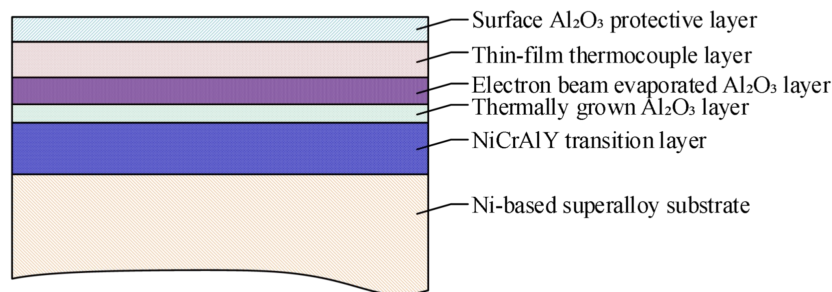

Figure 4. The structure schematic of NiCr-NiSi thin film thermocouple

The Ni-based superalloy substrate measures 100.0 mm × 40.0 mm × 2.0 mm. The NiCrAlY transition layer was prepared by magnetron sputtering, and the target material was used with a composition of $Ni_{67}Cr_{22}Al_{10}Y_1$ alloy rectangular target with the dimensions of 200 mm×300 mm×5 mm. The main process parameters are sputtering air pressure of 1.0 Pa, sputtering power of 1820 W, sputtering substrate temperature of 700 ℃, sputtering time of 2 h, and thickness of about 4.0 mm×4.0 mm. The thickness was about 4.0 μm, and the sample was put into a vacuum tube furnace for heat treatment in order to diffuse the metal Al in the transition layer of NiCrAlY to the surface to form a layer of metal Al with a thickness of about 200 nm, with the process parameters of vacuum degree of 0.5 Pa, temperature of 800 ℃, and heat preservation for 1 h. Then, the sample was put into a tube furnace for oxidization treatment to generate a layer of metal Al with a thickness of about 200 nm on the surface of the sample. Then, the sample was placed in a tube furnace for oxidation treatment to generate a layer of aluminum oxide with a thickness of about 200 nm on the sample surface, and the process parameters were 800 ℃ oxygen environment, holding temperature for 1 h, and then cooled with the furnace.

A layer of Al_2O_3 insulating layer with a thickness of approximately 4 μm was deposited on the sample surface by the electron beam evaporation method. The main process parameters were an air pressure of 5×10^{-2} Pa, a deposition temperature of 500 ℃, and an evaporation time of 1 hour. The NiCr-NiSi film thermocouple layer was prepared by the magnetron sputtering and mask patterning method. The target materials were $Ni_{90}Cr_{10}$ and $Ni_{97}Si_{10}$ alloys with dimensions of 100 mm × 5 mm. First, the thermocouple positive electrode NiCr film was deposited on the insulating layer, then the NiSi target and the corresponding mask for the positive electrode were replaced, and the thermocouple negative electrode NiSi film was sputtered to be prepared. The width of the prepared thermocouple was 5 mm, and the lengths were 80 mm and 25 mm respectively. The intersection of the two masks formed

a junction with a size of 5 mm × 2 mm. The main process parameters were a back-end vacuum degree of 3×10^{-3} Pa, a sputtering pressure of 0.5 Pa, and a sputtering time of 1 hour. Finally, a protective layer of Al_2O_3 with a thickness of approximately 1 μm was deposited on the thermocouple layer by the electron beam evaporation method.

A JSM-6530 scanning electron microscope (SEM) was used to characterize the surface morphology of the samples, an EDAX-Genesis X-ray spectrometer (EDS) was used to analyze the composition of the samples, a Bede-D1system X-ray diffractometer (XRD) was used to characterize the crystal structure of the samples, and an Agilent analyzer was used to test the insulating layer I-V curves. V curve. The static calibration of the thin film thermocouples was performed using a standard K-type thermocouple with a diameter of 0.05 mm. The thin film thermocouple nodes were extended into the heating furnace, and the temperature at the thin film thermocouple nodes was measured synchronously by fixing a sliver of standard thermocouples on the backside of the substrate opposite to the thin film thermocouple node position. The endpoints of the positive and negative electrodes of the film thermocouple are at room temperature outside the furnace, and the thermal potential of the film thermocouple is induced by the filament thermocouple to the test instrument, and the output of the thermal potential of the film thermocouple is recorded.

3. Results and discussion

3.1. NiCr-NiSi thin film sensor calibration test

3.1.1. Static calibration tests

In this paper, a self-designed and assembled temperature sensor static calibration system was used in the experiments to static calibrate the prepared improved NiCr-NiSi thin film thermocouple sensors. The main components of the static calibration system are FLUKE9144 temperature metering furnace, PLANCK-6190 type freezer, Yuden AI-701 artificial intelligence temperature controller, and computer. Among them, FLUKE-9144 temperature metering furnace, can provide accuracy ± 0.1 ℃, the temperature range of 20 ℃ -650 ℃ constant temperature field, a calibration can be set up to 8 calibration temperature points, built-in reference temperature metering device accuracy of up to +0.01 ℃. According to the thermocouple intermediate temperature law, if the cold end of the thermocouple is placed directly in the room temperature environment will lead to a reduction in the measured value of the thermoelectric potential. Therefore, it is necessary to keep the thermocouple cold end temperature at freezing point. The PLANCK-6190 freezer with an accuracy of ±0.05°C provides a freezing point constant temperature field for the cold end of the thin film thermocouple to ensure that the measured value of the computer during static calibration is a single-valued function of the readout value of the temperature metering oven.

The upper computer software is automatic data acquisition software written on LabVIEW 2015. This data acquisition software can communicate with the FLUKE-9144 temperature metering furnace through the RS232 serial port, send command codes to the furnace, and obtain the required data according to the parameters set on the software, such as the real-time furnace temperature, the execution state and the stability state and other information. The test data of the temperature sensor is automatically acquired by the software through the USB-RS485 converter.

The static calibration experiment process is as follows:

(1) The high-temperature transient temperature sensor leads were connected to the corresponding NiCr and NiSi compensation wire, in the compensation wire to select the appropriate location after insulation treatment into the freezing point of the thermostatic well, the other end of the compensation wire through the amplifier connected to the terminal of the data acquisition card.

(2) use access FLUKE9144 temperature measurement furnace K-type thermocouple as a standard thermocouple, thermocouple and to be calibrated high-temperature transient temperature sensors together into the measurement furnace well, and the measuring end of the two temperature sensors, is in the same position, in order to ensure that the temperature measurement data is reliable.

(3) Open the FLUKE9144 temperature measurement furnace power switch, set the temperature rise program. The prepared temperature sensor is designed to be used in the range of 50-650 ℃, so the static calibration of the temperature range of 50-650 ℃, starting from 50 ℃ every 50 ℃ to take a temperature calibration point, each temperature point to keep the temperature constant for 5min, record the measured thermoelectric potential value. The results of static calibration temperature T and thermopotential E of the improved NiCr-NiSi thin film thermocouple sensor are shown in Table 1.

Table 1. Data of temperature sensor static calibration

T/°C	E/mV	T/°C	E/mV
50	1.6623	400	21.3071
100	4.5280	450	23.5244
150	6.9787	500	26.4419
200	9.6758	550	28.7241
250	12.9435	600	30.8895
300	15.4590	650	32.5882
350	18.2599		

The least squares method was applied to linearly fit the static calibration data and the results are shown in Fig. 5. The relationship between the output thermopotential E of the temperature sensor and the temperature T at the measuring end is E=0.04834T-0.04405, with a Seebeck coefficient of 40.5 μV/C and a nonlinear error of 1.45%, which indicates that the linearity of the developed improved NiCr-NiSi thin-film thermocouple sensor is good.

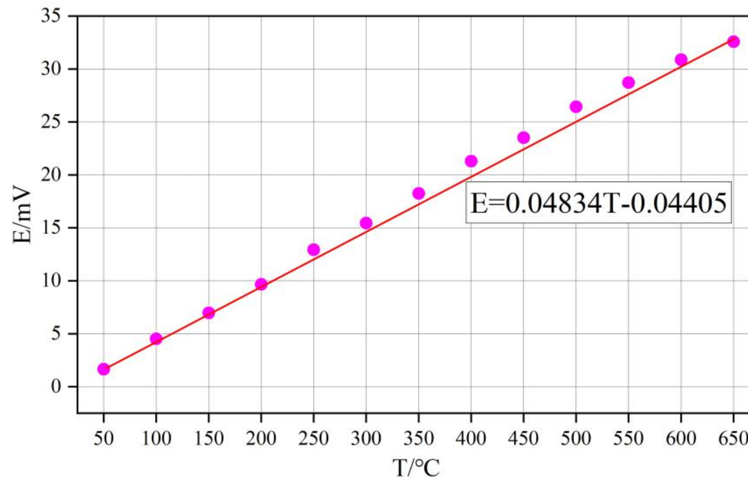

Figure 5. Static calibration data

3.1.2. Dynamic calibration tests

In practical applications, only a relatively perfect mathematical treatment of linear systems can be made at present, and it is difficult to make nonlinear system correction in dynamic testing. Therefore, in practice, often ignore the system's nonlinear and random changes and other complex factors, within a certain operating error allowed as a linear system P. In this paper, the improved NiCr-NiSi thin-film thermocouple sensor is a typical first-order system, in the process of analyzing its dynamic performance as a linear system.

The material parameters of each layer of the improved NiCr-NiSi thin film thermocouple sensor are shown in Table 2. The thermal conductivity of the Al_2O_3 protective film in the table is adopted as 4.54×10^{-4} $cal \cdot cm^{-1} \cdot s^{-1} \cdot k^{-1}$, and the rest of the data are adopted from the block material corresponding to the film material. Each parameter was substituted into the expression to obtain a time constant of about 38.5 μs.

Table 2. Parameters of each layer material of sensor

Materials of each layer of the sensor	Thermal conductivity k/ $cal \cdot cm^{-1} \cdot s^{-1} \cdot k^{-1}$	Thermal diffusivity a/ $m^2 \cdot s^{-1}$	Thickness θ/m
Al_2O_3 protective film	4.54×10^{-4}	7.52×10^{-4}	0.5×10^{-4}
NiCr	1.55×10^{-4}	3.60×10^{-4}	0.5×10^{-4}
NiSi	1.55×10^{-4}	3.60×10^{-4}	0.5×10^{-4}
Base	4.75×10^{-4}	8.25×10^{-4}	∞

The main components of the dynamic calibration system are Quantel laser Ultra 50 short pulse laser produced in the U.S.A. The basic parameters are repetition frequency 1-20 Hz, pulse width 8 ns, the

range of emitted laser energy 0.2-56.5 mJ, the value of emitted energy can be adjusted through the control handle, and the wavelength of the laser is 1050 nm. AD620 signal amplifier, amplification range 1~10,000, output voltage -10~10 V, input signal voltage range 100 μV-500 mV. 1~10000, output voltage -10~10 V, input signal voltage range 100 μV-500 mV. PXle-6366 data acquisition device, the maximum sampling frequency of 2MHz, data transmission resolution of 12-bit, with 64 data acquisition channels, embedded in the computer mainframe. The improved NiCr-NiSi film prepared in this paper has a thickness of about 500 nm, and larger laser pulse irradiation will lead to film damage and detachment, and the film will be damaged when the laser pulse energy is greater than 5 mJ after actual testing. The laser pulse energy is too small and will lead to the temperature rise curve is not obvious enough, after many tests, the selected parameters for the pulse laser energy value of 3mJ, set 1Hz as the pulse laser repetition frequency, the laser pulse width is fixed to 8ns, the sampling frequency of the NI acquisition card is set to 1MHz.

The dynamic calibration process of the improved NiCr-NiSi thin film thermocouple sensor is as follows:

(1) Fix the temperature sensor to be calibrated on the experimental bench stand;

(2) Turn on the Quantel laser Ultra 50 short pulse laser, adjust the position of the temperature sensor, so that the laser irradiates the thin film thermal contact to complete the positioning;

(3) Short pulse laser handle to set the laser delay time to irradiate the short pulse laser energy 3mJ;

(4) Irradiate the film hot contact with the set short-pulse laser to produce an instantaneous temperature rise in the temperature sensor.

(5) The existence of the temperature difference between the hot end and the cold end generates a thermoelectric potential in the temperature sensor, and the output signal is received by NI's PXIe-6366 data acquisition card after 10,000-fold amplification by a precision amplifier, and is ultimately uploaded to a computer.

The improved NiCr-NiSi thin-film thermocouple sensor belongs to the first-order inertial link, and the pulse width of the short-pulse laser used in the dynamic performance test is 8ns, which can be regarded as a pulse excitation signal and can be used as the pulse input of the first-order system compared with the microsecond dynamic response time of the thin-film thermocouple. The curves obtained from the dynamic calibration experiments are shown in Fig. 6. The measured time constant of the improved NiCr-NiSi thin-film thermocouple sensor is 85.05 μs, which has some deviation from the theoretically calculated time constant of 38.5 μs. The reason for this is that during the theoretical calculation process, ideal boundary conditions are used in the establishment of the differential equations of thermal conductivity, which differ from the actual temperature measurement of temperature sensors, and these lead to the smaller theoretically calculated value compared with the measured value. The dynamic calibration system circuit has signal interference and hysteresis, which can lead to the experimentally measured time constant is large.

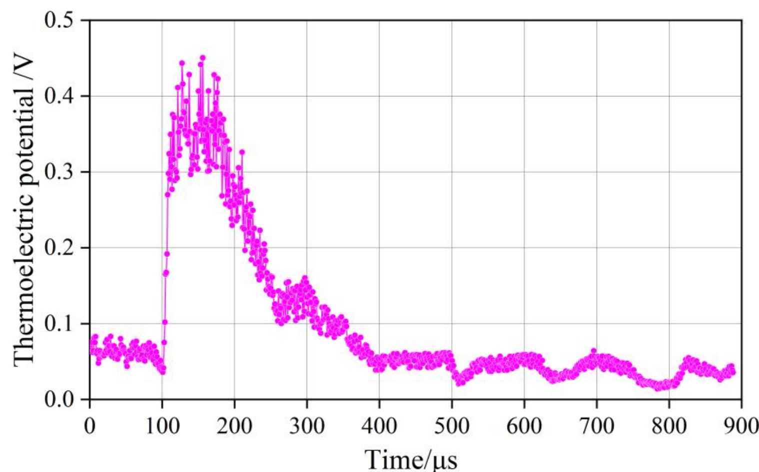

Figure 6. Dynamic calibration curve of high temperature transient sensor

3.2. Compositional Analysis of NiCr/NiSi Thin Film Thermocouples

3.2.1. Chemical composition analysis

In addition to the impurities in the films, the chemical composition of the NiCr and NiSi thermoelectric electrodes should be considered, which is changed by selective sputtering of the target.

In order to avoid interfering signals from the substrate, EDS measurements of NiCr and NiSi thermoelectric electrodes with a thickness of 500 nm are shown in Tables 3 and 4, and other thicknesses are similar. It can be seen that no other impurity elements were detected except for C and O elements. Due to the EDS measurements, the C and O elements are mainly from organic pollutants which are absorbed into the film surface. Therefore, according to the EDS results, the NiCr thermoelectric electrode consists of the elements Ni and Cr with the atomic ratios of Ni/Cr = 88.93/12.25, respectively, and the NiSi thermoelectric electrode consists of the elements Ni and Si with the atomic ratios of Ni/Si = 90.34/7.25, respectively, which is in agreement with the results of the thermoelectric electrodes of the sputtering target and the standard K-type thermocouple, and it can be then established that the above two problems are not caused by the chemical composition in the thermoelectric electrode.

Table 3. NiCr thermoelectric electrode

Element	Characteristic X-ray energy (keV)				Standard reference	at. %	Ni/Cr atom ratio
	K_α	K_β	L_α	L_β			
C	0.275	--	--	--	$CaCO_3$	15.15	
O	0.533	--	--	--	SiO_2	6.73	$\frac{88.93}{12.25}$
Cr	5.509	6.053	0.597	0.593	Cr	9.73	
Ni	7.552	8.304	0.869	0.892	Ni	68.34	
		Total				100.00	

Table 4. NiSi thermoelectric electrode

Element	Characteristic X-ray energy (keV)				Standard reference	at. %	Ni/Cr atom ratio
	K_α	K_β	L_α	L_β			
C	0.275	--	--	--	$CaCO_3$	16.17	
O	0.533	--	--	--	SiO_2	7.42	$\frac{90.34}{7.25}$
Si	1.733	1.835	--	--	SiO_2	6.61	
Ni	7.552	8.304	0.869	0.892	Ni	70.39	
		Total				100.00	

3.2.2. Chemical bond structure analysis

The full spectrum of NiCr before and after XPS test cleaning is shown in Fig. 7. Comparing the two spectral lines, the yellow line is the XPS spectrum of the film surface before cleaning, and it can be seen that the composition of the film surface contains Ni, Cr, and C. At a lower Ar^+ accelerating voltage and shorter cleaning time, the surface of the film is bombarded with Ar^+ bombarded the film surface for 10 min, and the composition of the cleaned film contained only Ni and Cr without C, as shown in the green chromatographic line. Except for the characteristic peaks of C 1s and O 1s, the positions of the characteristic peaks of other elements in the two spectral lines are identical. After surface removal, the peak intensity of NiCr is significantly enhanced. The peaks belonging to C and O appearing at the surface are due to air contamination of the film surface, and this peak no longer appears after the surface is cleaned, which indicates that the composition of the improved NiCr/NiSi film contains NiCr without C and O. The peaks belonging to C and O appearing at the surface are due to air contamination of the film surface.

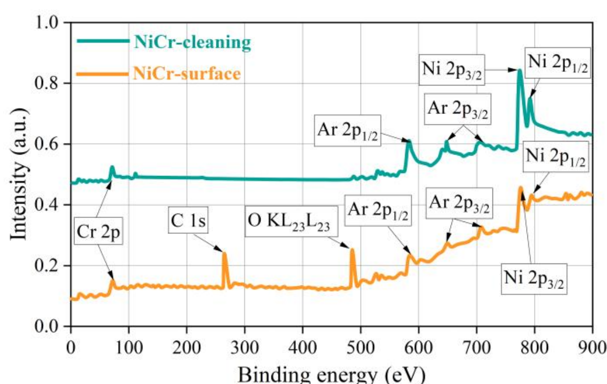

Figure 7. XPS spectral lines of NiCr films before and after cleaning

The full spectrum of NiSi before and after XPS test cleaning is shown in Fig. 8. Comparing the two spectral lines, the yellow spectral line is the XPS spectral line of the film surface before cleaning, which shows that the composition of the film surface contains Ni, Si and C. The XPS spectral line of the film surface before cleaning is shown in Fig. 8. At a lower Ar^+ accelerating voltage and a shorter cleaning time, the surface of the film was bombarded with Ar^+ for 10 min, and the composition of the cleaned film contained only Ni, Si and no C as shown in the green chromatographic line. Except for the characteristic peaks of C 1s and O 1s, the positions of the characteristic peaks of other elements in the two spectral lines are identical. After the surface was cleaned, the peak intensity of NiSi was significantly enhanced. The peaks belonging to C and O appearing at the surface are due to the air pollution on the film surface, and the peaks no longer appear after the surface is cleaned, which indicates that the composition of the improved NiCr/NiSi film contains NiSi without C and O. The peaks belonging to C and O appear at the surface due to the air pollution on the film surface, and the peaks no longer appear after the surface is cleaned.

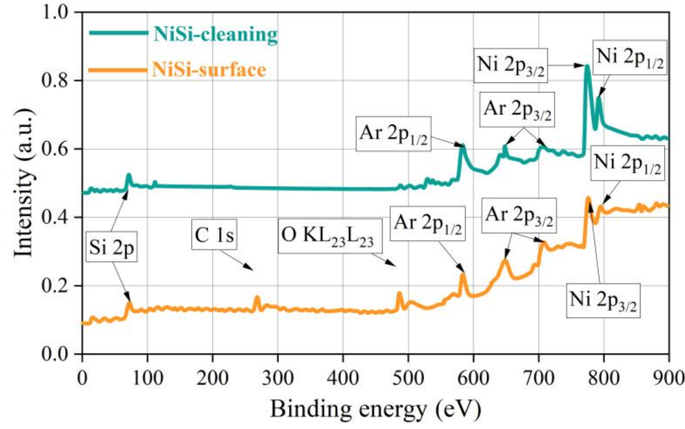

Figure 8. XPS spectral lines of NiSi film before and after cleaning

3.3. Discussion

In this paper, it is found that the Seebeck coefficient of the prepared improved NiCr-NiSi thin film thermocouple is 40.5 μV/K, which is slightly lower than that of the Seebeck coefficient of the NiCr/NiSi standard thermocouple (41 μV/K). The static calibration system, mentioned earlier, has different Seebeck coefficients for different calibration methods. Literature research revealed that the calibration method used by most researchers is to place the entire NiCr-NiSi thin film thermocouple into the calibration furnace with the leads connected to the NiCr and NiSi compensation wires, respectively. The Seebeck coefficients obtained by this calibration method are close to the standard Seebeck coefficients, which are the Seebeck coefficients of the calibrated NiCr and NiSi compensation wires, because both the hot end and the lead end are put into the calibration furnace, and because of the small size of the thermocouples, the hot end and the lead end are too close to each other, and in the calibration the hot end and the lead end are in the same temperature field, and the temperature between them is the same ($T_{hot} = T_{pad}$).

According to the third conductor law of thermocouple, the hot end and lead end temperatures are in the same temperature field, which does not generate electric potential and there is no Seebeck coefficient, so the Seebeck coefficients of NiCr and NiSi compensation wires calibrated by this method are in error. Calibration of the static calibration procedure using the third calibration method, i.e., calibration of the modified NiCr-NiSi thin film thermocouple with the same film thickness of 500 nm in this paper results in 8.05 μV/°C, which is accurate. Using the third static calibration procedure mentioned in this paper, where only the hot end of the NiCr/NiSi thin-film thermocouple is placed in the calibration furnace and the lead end is connected to the copper compensation wire, consider ΔT_{pad}^{hot}. Calibration using this method results in accurate Seebeck coefficient values that can be reliably applied for accurate temperature measurement of UAV engines.

4. Conclusion

In this paper, the preparation and study of high-temperature thin-film thermocouples were carried out in the context of complex structure and temperature monitoring inside the engine of an unmanned aerial vehicle (UAV). The conclusions are summarized as follows:

(1) An improved NiCr-NiSi thin-film thermocouple sensor for measuring the precise temperature of UAV engines has been successfully developed, and Al_2O_3 insulating thin film, NiCr- NiSi thermal electrode film and NiCrAlY protective film were prepared. The surface morphology of Al_2O_3 insulating films was observed by SEM, and it was found that the surface was dense, uniform and of good continuity, which meets the insulating requirements of thermocouples.

(2) Using the self-developed dynamic and static calibration system, the developed special structure thin film sensor is calibrated. The results show that the improved NiCr-NiSi thin-film sensor has good linearity, high sensitivity and fast response speed, with a Seebeck coefficient of 40.5 μV/K, a nonlinear fitting error of only 1.45% and a dynamic response time of 85.05 μs.

(3) The prepared improved NiCr-NiSi thin-film thermocouple sensor has good thermal stability and high temperature resistance, which can meet the needs of transient temperature testing in the range of room temperature~650C.

About the Author

Jiayi Sun, female, Han ethnicity, from Heilongjiang Province, currently a freshman at Northeast University. Major: Materials Science and Engineering (a Sino-foreign cooperative program).

References

1. Wang, Y., Shi, Y., Cai, M., Xu, W., Pan, T., & Yu, Q. (2019). Study of fuel-controlled aircraft engine for fuel-powered unmanned aerial vehicle: Energy conversion analysis and optimization. IEEE Access, 7, 109246-109258.
2. Cirigliano, D., Frisch, A. M., Liu, F., & Sirignano, W. A. (2018). Diesel, spark-ignition, and turboprop engines for long-duration unmanned air flights. Journal of Propulsion and Power, 34(4), 878-892.
3. LAGHARI, Asif Ali, et al. Unmanned aerial vehicles: A review. Cognitive robotics, 2023, 3: 8-22.
4. Tahir, A., Böling, J., Haghbayan, M. H., Toivonen, H. T., & Plosila, J. (2019). Swarms of unmanned aerial vehicles—A survey. Journal of Industrial Information Integration, 16, 100106.
5. Greene, B. R., Segales, A. R., Waugh, S., Duthoit, S., & Chilson, P. B. (2018). Considerations for temperature sensor placement on rotary-wing unmanned aircraft systems. Atmospheric Measurement Techniques, 11(10), 5519-5530.
6. Fu, X., Lin, Q., Peng, Y., Liu, J., Yang, X., Zhu, B., ... & Chen, S. (2020). High-temperature heat flux sensor based on tungsten–rhenium thin-film thermocouple. IEEE Sensors Journal, 20(18), 10444-10452.
7. Xie, Y., Cui, Y., Wang, H., & Feng, W. (2024). Research on a dedicated thin-film thermocouple testing system for transient temperature measurement. Measurement Science and Technology, 35(8), 085117.
8. Zhao, X. H., Wang, Y. R., Chen, Y. Z., Jiang, H. C., & Zhang, W. L. (2017). Enhanced thermoelectric property and stability of NiCr–NiSi thin film thermocouple on superalloy substrate. Rare Metals, 36(6), 512-516.
9. Sun, Y., Liu, Z., Hao, Y., Liu, J., Wang, Q., Wang, H., ... & Ding, W. (2024). Preliminary investigation of thermoelectric electromotive force oscillation of NiCr/NiSi thin film thermocouple in dynamic calibration. Small, 20(23), 2308002.
10. Liu, Z., Shen, K., Wang, X., Zhang, M., Cheng, Y., Wang, B., ... & Wang, Z. (2025). Experimental Study on Influencing Factors of Seebeck Coefficient by Using NiCr/NiSi Thin-Film Thermocouple Prepared and Calibrated. physica status solidi (a), 222(6), 2400653.
11. Liu, Z., Chang, B., Li, J., Chen, Y., Wang, X., Rong, Z., ... & Ding, W. (2025). Preliminary monitoring and observation of fuel cell temperature characteristics by using NiCr-NiSi thin-film thermocouple. Micromachines, 16(6), 639.
12. Liu, Z., Guo, T., Cheng, Y., Wang, B., Shen, K., Hu, K., ... & Ding, W. (2024, March). Mechanism of Seebeck coefficient variation at the output of NiCr/NiSi thin film thermocouple with different wires. In Journal of Physics: Conference Series (Vol. 2724, No. 1, p. 012001). IOP Publishing.

13. Cui, Y., Liu, Q., Wang, L., Ding, W., Wang, X. V., Liu, Y., & Li, D. (2018). Research on milling temperature measuring tool embedded with NiCr/NiSi thin film thermocouple. Procedia CIRP, 72, 1457-1462.
14. Chen, Y., Chen, Q., Yin, Y., Yang, Y., Wang, Y., Kong, G., ... & Liu, Z. (2025). Accurate temperature measurement of new energy vehicle engine by using NiCr-NiSi thin film thermocouple. Journal of Mechanical Science and Technology, 39(3), 1469-1476.